



Contents lists available at SciVerse ScienceDirect

Surface & Coatings Technology

journal homepage: www.elsevier.com/locate/surfcoat

Wear and corrosion performance of WC-10Co4Cr coatings deposited by different HVOF and HVOF spraying processes

Qun Wang^{a,*}, Shiyong Zhang^b, Yingliang Cheng^a, Jing Xiang^a, Xinqi Zhao^a, Guibin Yang^c

^a College of Materials Science and Engineering, Hunan University, Changsha, Hunan 410082, PR China

^b Department of Biological and Environmental Science, Changsha University, Hunan 410003, PR China

^c Ganzhou Achteck Tool Technology Co., Ltd., Ganzhou, Jiangxi 341300, PR China

ARTICLE INFO

Article history:

Received 7 September 2012

Accepted in revised form 27 December 2012

Available online xxx

Keywords:

HVOF

WC-CoCr coating

Abrasive wear

Sliding wear

Electrochemical corrosion

ABSTRACT

This study compares three types of WC-10Co4Cr coatings deposited with high-velocity oxygen fuel (HVOF) and high-velocity air fuel (HVOF) spraying processes. The experimental results indicated that the decarburisation of the WC in the WC-10Co4Cr coating was dramatically influenced by the spraying equipment, and the non-WC phase content in the as-sprayed coatings greatly influenced their performances. The HVOF-sprayed WC-10Co4Cr coating revealed the lowest degree of decarburisation, achieving the best properties in terms of hardness, fracture toughness, abrasive and sliding wear as well as electrochemical corrosion resistance when compared to the two HVOF-sprayed WC-10Co4Cr coatings.

© 2013 Elsevier B.V. All rights reserved.

1. Introduction

Tungsten carbide (WC)-based powders are widely used in high-velocity oxygen fuel (HVOF) spraying to produce dense coatings with high hardness and excellent wear resistance [1,2].

Although substantial improvement in coating properties can be obtained when spraying WC-cermets using the HVOF process instead of a plasma spraying technique, various degrees of the WC decarburisation still occur during the deposition process. A large number of researchers have reported that the decarburisation of WC has a detrimental effect on the abrasive wear resistance of coatings due to the increasing brittleness and the decrease in hard particle content [2–5]. Thus, there is a need for a spraying equipment that operates at a much lower temperature and generates a higher flame velocity. A high-velocity air fuel (HVOF) system that uses gas or liquid fuel and compressed air (not oxygen) for combustion has been explored to meet this need [4–8], and it has been found that depositing WC-based coatings by the HVOF spraying process can reduce the production cost due to the use of air instead of pure oxygen, while greatly decreasing the degree of WC [4,5,9] or Cr₃C₂ [10] decarburisation as a result of much lower flame temperature. Jacobs et al. [4,5] found that HVOF-sprayed WC-based coatings exhibited a higher degree of hardness and improved sliding wear performance without decarburisation as compared to the HVOF method and attributed the higher wear resistance to the greater retention of WC particles in the former coating type.

They also suggested that much more research was needed to compare performance of coatings deposited by the HVOF and HVOF spraying processes, especially for HVOF guns that use oxygen and kerosene for combustion. Furthermore, although the corrosion performance of HVOF-sprayed WC/Co(Cr) was studied in detail in the literature [11–15], the corrosion performance of the HVOF-sprayed WC/Co(Cr) coating has not yet been reported.

In this study, three WC-10Co4Cr coatings were deposited with similar powder using Kermetico's AK 07 HVOF spray system (AK) operating with propane and compressed air, the Praxair's JP8000 HVOF spray system (JP) operating with kerosene and pure oxygen, and the Deloro Stellite's Jet Kote® III HVOF spray system (JK) operating with propylene and pure oxygen. The microstructures, mechanical properties, abrasive and sliding wear as well as the electrochemical corrosion resistances of the as-sprayed coatings were investigated.

2. Experiment

2.1. Materials

The WC-10Co4Cr powder (Ganzhou Achteck Tool Technology Co., Ltd, China) was sprayed on a low-carbon steel substrate using HVOF and HVOF equipment. The same lot of the material was spray-dried and agglomerated, sintered into sprayable particles in the same process, and then sieved to obtain two powder types with different size distributions. Fine powder with the particle size of 5–30 μm was used for the HVOF process and the coarse powder with the particle size of 15–45 μm was used for the two HVOF processes. These two WC-10Co4Cr powders had similar chemical compositions (mass

* Corresponding author. Tel.: +86 13787113453; fax: +86 731 88821611.
E-mail address: 13787113453@163.com (Q. Wang).

percentages: W: 80.29%, C: 5.23%, Co: 10.28%, and Cr: 3.96%) and the same WC sizes (mean size of approximately 1.5 μm). The WC-10Co-4Cr powder typical micrograph is presented in Fig. 1.

As observed in Fig. 1, the spray powder particles were of ideal spherical shape. The powder had excellent flowability and was well fed through the spray systems.

2.2. Preparation of HVOF coatings

Prior to the spraying process, rectangular ($200 \times 57 \times 5 \text{ mm}^3$) low carbon steel samples were degreased and grit blasted with 60 meshes of Al_2O_3 . The approximately 0.3 mm thick WC-10Co-4Cr coatings were deposited on these substrates using the AK 07 HVOF (Kermetico, USA), JP8000 HVOF (Praxair Surface Technologies, USA) and Jet Kote III HVOF (Deloro Stellite, USA) spray guns, respectively. All of the spray systems were equipped with mass flow metres, and the spraying parameters used in this work were provided by the spray gun manufacturers. The spraying equipment reference, parameters and coating codes are presented in Table 1.

The spraying angle was 90° and the temperatures of the substrates during spraying were kept below 150°C using compressed air cooling.

2.3. Characterisation

X-ray diffraction (XRD) analysis of the powder and coatings was performed with a RigakuD/max-2550 diffraction metre using Cu-K α radiation. The ratio of main peak height of W_2C to WC (W_2C peak at $d = 2.276 \text{ \AA}$ [$2\theta: 39.6^\circ$] and WC peak at $d = 1.883 \text{ \AA}$ [$2\theta: 48.3^\circ$]) was used as an indication of the extent of WC decarburization in the as-sprayed coatings [16]. Scanning electron microscopy (SEM) images of the cross-sections as well as the coatings' worn corroded surfaces were obtained using the FEI-Quanta200 equipped with the EDS system. The porosity measurements were performed on the coating cross-sections using the image analysis system of the Zeiss optical microscope. The presented porosity data were the average of ten measurements. The hardness measurements were performed on the coating cross-sections at loads of 0.3 kg and 5 kg, and an average of ten readings were reported. Cracks parallel to the substrate appeared on the cross-sections of the as-sprayed coatings under the load of 5 kg. The coating fracture toughness value was calculated using the

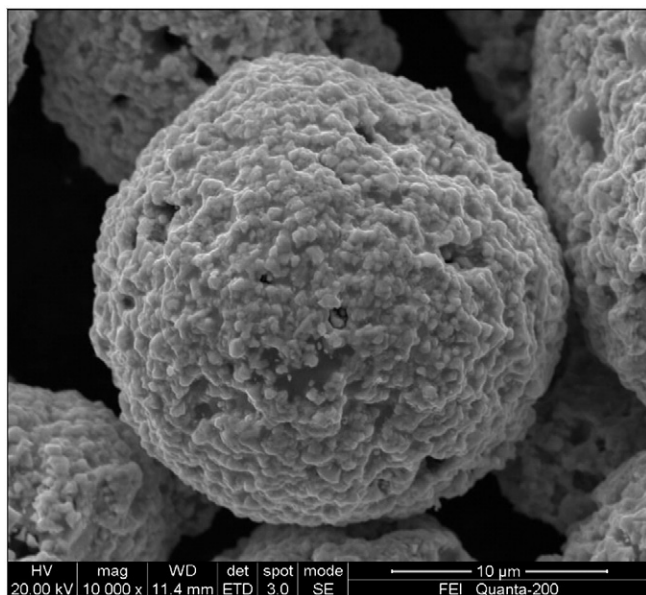


Fig. 1. Micrograph of the WC-10Co4Cr powder.

Table 1
Coating codes, spraying equipment and parameters for the three WC-10Co4Cr coatings.

Coating code	AK	JP	JK
Gun	AK 07 (HVOF)	JP8000 (HVOF1)	Jet Kote III (HVOF2)
Combustion mixture	Propane pressure:	Kerosene:	Propylene:
	0.52 MPa	22.7 L/min	64.2 L/min
	Air pressure:	Oxygen:	Oxygen:
	0.61 Mpa	873.0 L/min	481.4 L/min
Feed rate (g/min)	75	75	55
Spraying distance (mm)	150	380	180
Carrier gas flow (L/min)	14.16	10.85	26.90
Horizontal velocity (mm/s)	1000	1000	1500
Vertical step (mm)	2.5	5	2.5

length of the indentations and the cracks according to the Evans and Wilshaw equation (adopted in our previous research [17]).

2.4. Abrasion and sliding wear tests

2.4.1. Abrasion wear tests

The coated specimens, with dimensions of $57 \times 25 \times 5.3 \text{ mm}^3$, were tested using the wet sand rubber wheel abrasion tester (MLS-225, Dynamic balance testing machine Co. Ltd., Zhangjiakou, China) [1,17]. The steel wheel covered in vulcanised rubber, with a Shore hardness of 72, was turned against the test specimen at the load of 100 N. The rotation speed of the rubber wheel was 240 rpm. The tribological pair was submerged in a mixture of 40–70 mesh quartz sand (1.5 kg) and fresh water (1 kg), and the abrasive slurry used in the process was not recycled. The test lasted for 6500 revolutions, the first 500 of which were performed only to accommodate the system and were not counted in the wear measurements. Before and after the test all coatings were ultrasonically cleaned with acetone for 5 min and then dried by the hot air stream. The samples loss of mass was measured using the FA1004 electric balance with an accuracy of 0.1 mg.

2.4.2. Sliding wear tests

The sliding wear behaviour and friction of the as-sprayed coatings were characterised using a reciprocating ball-on-block UMT-3MT tribometer (Center for Tribology, Inc., Campbell, United States) at room temperature and the relative humidity of 55–60% under dry sliding conditions. The zirconia ball of 9.525 mm diameter was used as the counter body. All tests were performed under a load of 50 N, the sliding speed of 0.075 m/s and the total time of 1800 s. The friction coefficient and sliding time were recorded automatically during the tests.

2.5. Electrochemical corrosion tests

The electrochemical behaviour of the coated samples at room temperature was examined in the aerated and unstirred 3.5 wt.% NaCl solution using the CHI660B DSP workstation (ChenHua Instruments Co. Ltd., Shanghai, China). The sample was mounted in the electrochemical cell with an area of 1.0 cm^2 exposed to the electrolyte. In the electrochemical tests, a saturated calomel electrode (SCE) and platinum (Pt) were used as the reference and counter electrodes, respectively. The electrochemical tests included measurement of the open-circuit potential and potentiodynamic polarisation tests. The open-circuit potential was measured after the coating surface was immersed in 3.5 wt.% NaCl solution for 30 min to stabilise its potential. The samples were potentiodynamically polarised anodically, and the tests were performed at a scanning rate of 0.5 mV s^{-1} . At least two sets of measurements were performed on each sample to ensure the reproducibility of the results.

3. Results

3.1. Phase compositions

Fig. 2 shows the XRD results for WC-10Co4Cr powder and coatings produced by the AK 07, JP8000 and Jet Kote III spraying systems.

Fig. 2 shows that the AK coating deposited by the HVAF spraying process nearly had showed the same phase composition as its feedstock powder, being composed of a main WC and minor $\text{Co}_3\text{W}_3\text{C}$ and crystal Co phases and exhibiting nearly no decarburisation. The JK coating sprayed by the Jet Kote III HVOF equipment exhibited the most severe decarburization, with the high intensity of the W_2C and even the presence of metallic W peaks. The phase composition of the JP coating deposited by the JP8000-HVOF system was composed of a main WC and minor W_2C phase and exhibited slight decarburisation. In addition, the Co peak disappeared and certain amorphous peaks appeared in the two HVOF-sprayed coatings due to the rapid cooling rate of the fully molten sprayed particles, which impacted the substrate during the spraying process [17].

3.2. Microstructure of the WC-10Co4Cr coatings

Typical cross-sectional BSE images of the AK, JP and JK WC-10Co4Cr coatings are shown in Fig. 3.

As observed in Fig. 3, the two HVOF-sprayed coatings exhibited some degree of laminar microstructures. According to their cross-sectional BSE images, these thin white strips with some high light particles in the JP and JK coatings parallel to the interface between the coating and substrate may be the mixtures of the amorphous matrix and W_2C , W and complex carbides. Formation of these phases can be attributed the dissolution of WC into the molten binder phase during spraying. According to Stewart et al. [18], some carbon elements in the molten Co binder reacts with oxygen and generates CO or CO_2 gas, while the other carbon elements remain in the Co binder and appear in the form of elementary carbon elements or carbon compounds generated by precipitation reactions when the molten Co binder solidifies into a solid state. In addition, some micro-cracks were found among the splats of the HVOF coatings, especially in the JK coating, which could be attributed to excessive shrinkage rates of the large number of fully molten particles being deposited on the substrate at a rapid cooling rate. Additionally, as for the JK coating, the grain size of the WC decreased with an increase in the level of WC decarburization, mainly through dissolution into the Co/Cr binder (Fig. 3f). As for the HVAF-sprayed WC-10Co4Cr coating, no apparent white laminar structure could be found in its cross-sectional images because nearly no W_2C or W phase was generated during the low-temperature-flame HVAF spraying process.

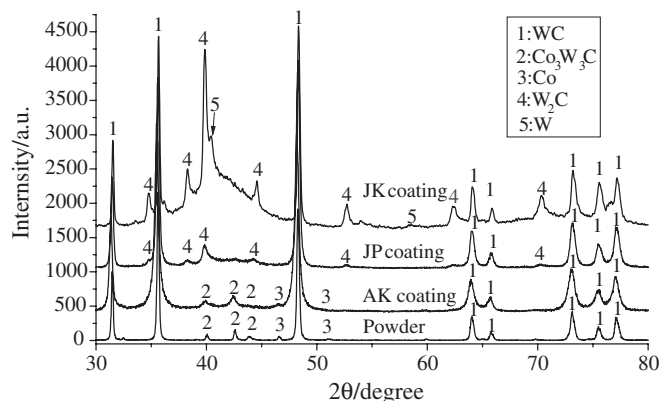


Fig. 2. XRD patterns of the WC-10Co4Cr powder and coatings.

3.3. Performance of the WC-10Co4Cr coatings

3.3.1. Mechanical properties of the WC-10Co4Cr coatings

The data for hardness, porosity, fracture toughness and the main peak height ratio of W_2C to WC phases are presented in Table 2 for all of the WC-10Co-4Cr coatings under investigation.

Table 2 shows that the AK coating deposited by the HVAF process exhibited the highest hardness and fracture toughness and the lowest porosity. The JK coating showed the lowest hardness and fracture toughness and the highest porosity, while the properties of the JP coating were in between those of the AK and JK coatings.

3.3.2. Wear and electrochemical corrosion resistance of the WC-10Co4Cr coatings

The data for abrasive wear rate, sliding wear track width, friction coefficient, open circuit potential and corrosion current density for the WC-10Co4Cr coatings are presented in Table 3.

According to the results in Table 3, the AK coating exhibited the highest abrasive and sliding wear resistance, friction coefficient and open circuit potential, but it also had the lowest corrosion current density, whereas the JK coating exhibited the poorest performance except in terms of its friction coefficient which was the lowest. The performance of the JP coating was generally located in between that of the AK and JK coatings.

4. Discussion

4.1. Decarburisation mechanism of the HVAF- and HVOF-sprayed WC-10Co4Cr coatings

Numerous authors have reported that WC grains experience different degrees of decarburisation during HVOF process [16–23]. The decarburisation transformation from WC to W_2C , W and amorphous Co–W–C phases occurred as a result of direct oxidation on the surface of the solid WC according to the literature [19,20]. However, more and more researchers [17,18,21–23] have suggested that the indirect oxidation of WC, which occurs when molten liquid cobalt is used as a medium, is the primary model of decarburisation. The decarburisation mechanism discussed above can be used to explain the WC decarburisation process observed in this study.

The AK coating deposited by the HVAF spraying process showed almost no decarburisation, which was attributed to its lower temperature compared to the two HVOF spraying processes. As for the two HVOF-sprayed coatings, their level of decarburisation was also very different. The powder experienced a higher temperature and longer residence time in the plume when its entrance was located in the combustion chamber of the Jet Kote III spray gun than in the lower temperature flame when the powder entrance was in the expanded nozzle after the combustion chamber of the JP8000 spray gun. This could explain the higher degree of WC decarburisation in the JK coating. Zhang et al. [24] have also found that liquid-fuelled HVOF spraying systems generate lower particle temperatures and higher particle velocities during spraying than the gas-fuelled HVOF systems.

Additionally, Fig. 2 shows that the metastable $\text{Co}_3\text{W}_3\text{C}$ phase existing in the initial feedstock powder, decomposed in a high temperature flame during the two HVOF spraying processes while was retained in the AK coating, which was also the result of the relatively low temperature in the HVAF spraying process. The $\text{Co}_3\text{W}_3\text{C}$ phase can usually be observed in the WC-10Co4Cr powder, but hardly ever in WC-12Co powder [4,5], which can be attributed to the deficiency of carbon elements in the powder. Because the carbon element in WC is prone to react with Cr and may generate some chrome carbide during the WC-10Co4Cr powder sintering process, the traces of $\text{Co}_3\text{W}_3\text{C}$ generation will occur in the feedstock powder.

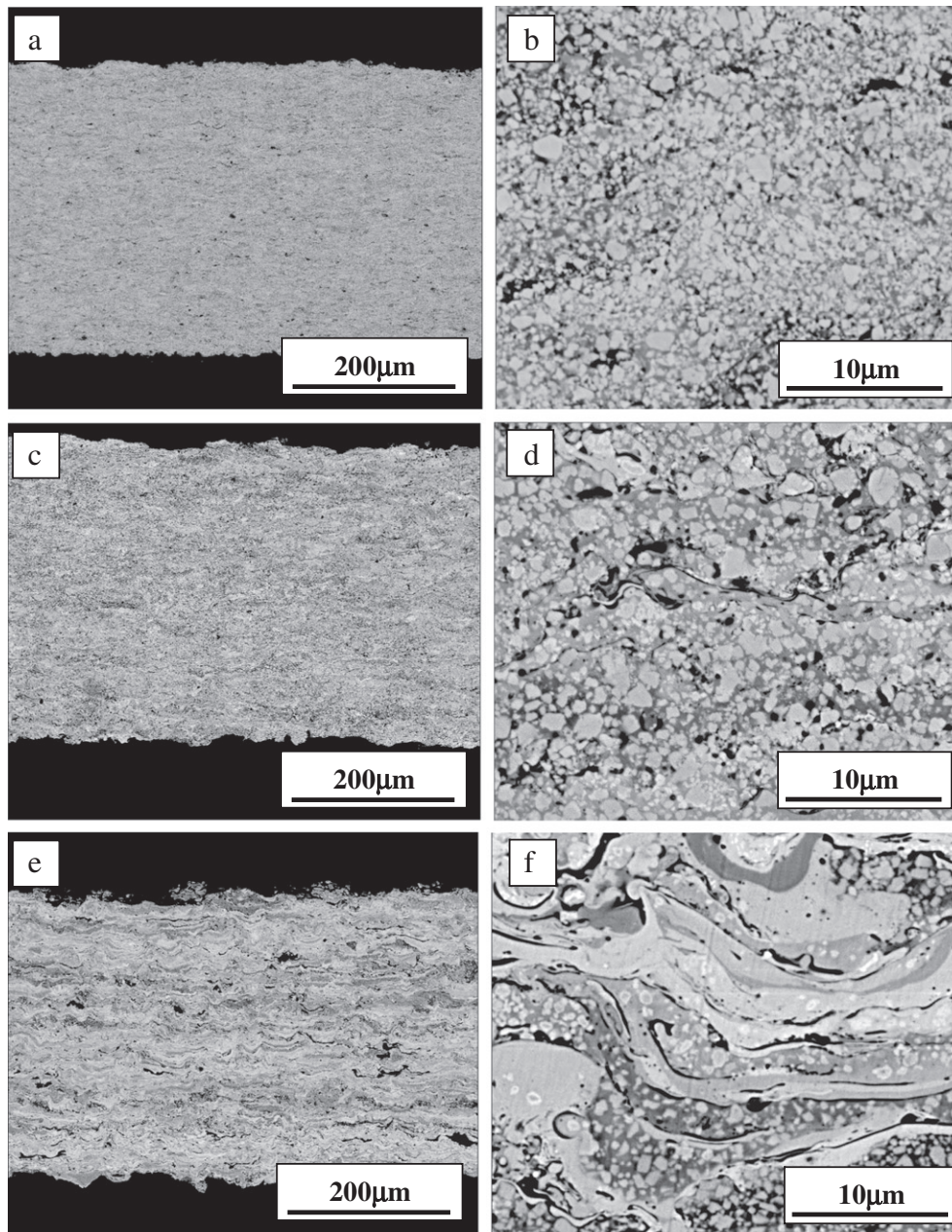


Fig. 3. Cross-sectional microstructures of the (a and b) AK, (c and d) JP and (e and f) JK coatings.

4.2. Fracture toughness of the HVOF- and HVOF sprayed WC-10Co4Cr coatings

The fracture toughness of the coatings was tested using the indentation method. Typical indent micrographs on the cross-sections of the AK, JP and JK coatings are shown in Fig. 4.

Table 2

Hardness, fracture toughness and the main peak height ratio of W₂C to WC phases in the three WC-10Co4Cr coatings.

Coating	Hardness		Porosity (%)	Fracture toughness (MPam ^{1/2})	Ratio of W ₂ C to WC
	HV0.3	HV5			
AK	1362.6 ± 97.6	1268.2 ± 27.6	0.3	5.97 ± 0.68	~0
JP	1289 ± 107.6	1169.1 ± 47.3	0.6	4.87 ± 0.59	0.12
JK	1047 ± 112.3	932.4 ± 57.6	1.7	3.01 ± 0.55	0.70

As Fig. 4 shows there are many longer cracks after indentation in the cross-sections of the JK coating than in the AK coating. Furthermore, the cracks in the JK coating propagated mainly through the W-rich binder regions (white-colour areas) along the splats, which were not present on the micrographs of the AK coating. Chivavibul et al. [25] have also found similar phenomena and attributed it to the high brittleness of the amorphous binder as well as to the poor cohesion and micro-cracks that originally exist within the splats in the JK coating.

4.3. Abrasive wear mechanism of the HVOF- and HVOF-sprayed WC-10Co4Cr coating

The literature has proposed an abrasive wear mechanism for WC-Co(Cr) coatings as follows: “(i) extrusion of the binder phase and removal by plastic deformation and fatigue, (ii) undermining of the particles and subsequent particle pull-out, (iii) micro-cutting,

Table 3

Abrasive wear rate, sliding wear trace width, friction coefficient, open circuit potential and corrosion current density of the three WC-10Co4Cr coatings.

Coating	Abrasive wear rate ($\times 10^{-6}$ g/m)	Sliding wear		Electrochemical corrosion	
		Wear trace width (mm)	Friction coefficient	Open circuit potential (V)	Corrosion current density ($\times 10^{-6}$ A/cm ²)
AK	3.76 ± 0.26	0.873 ± 0.071	0.656 ± 0.176	-0.405 ± 0.049	2.118 ± 0.321
JP	6.05 ± 0.48	0.986 ± 0.082	0.626 ± 0.188	-0.433 ± 0.051	3.316 ± 0.413
JK	18.72 ± 1.13	1.427 ± 0.095	0.554 ± 0.193	-0.587 ± 0.059	14.896 ± 1.35

(iv)carbide grain fracture and (v) delamination of the coating" [1,17]. These wear mechanisms can generally explain the wear process of the WC-10Co4Cr coatings in this study, too. Herewith, the coatings with different degrees of decarburization exhibited different dominant wear mechanism.

The typical images of worn surfaces of the AK, JP and JK coatings are shown in Fig. 5.

The low magnification images of the worn surfaces (Fig. 5a, c and e) indicate that the AK and JP coatings exhibited smoother worn surfaces than the JK coating. There were many grooves and pits on the surface

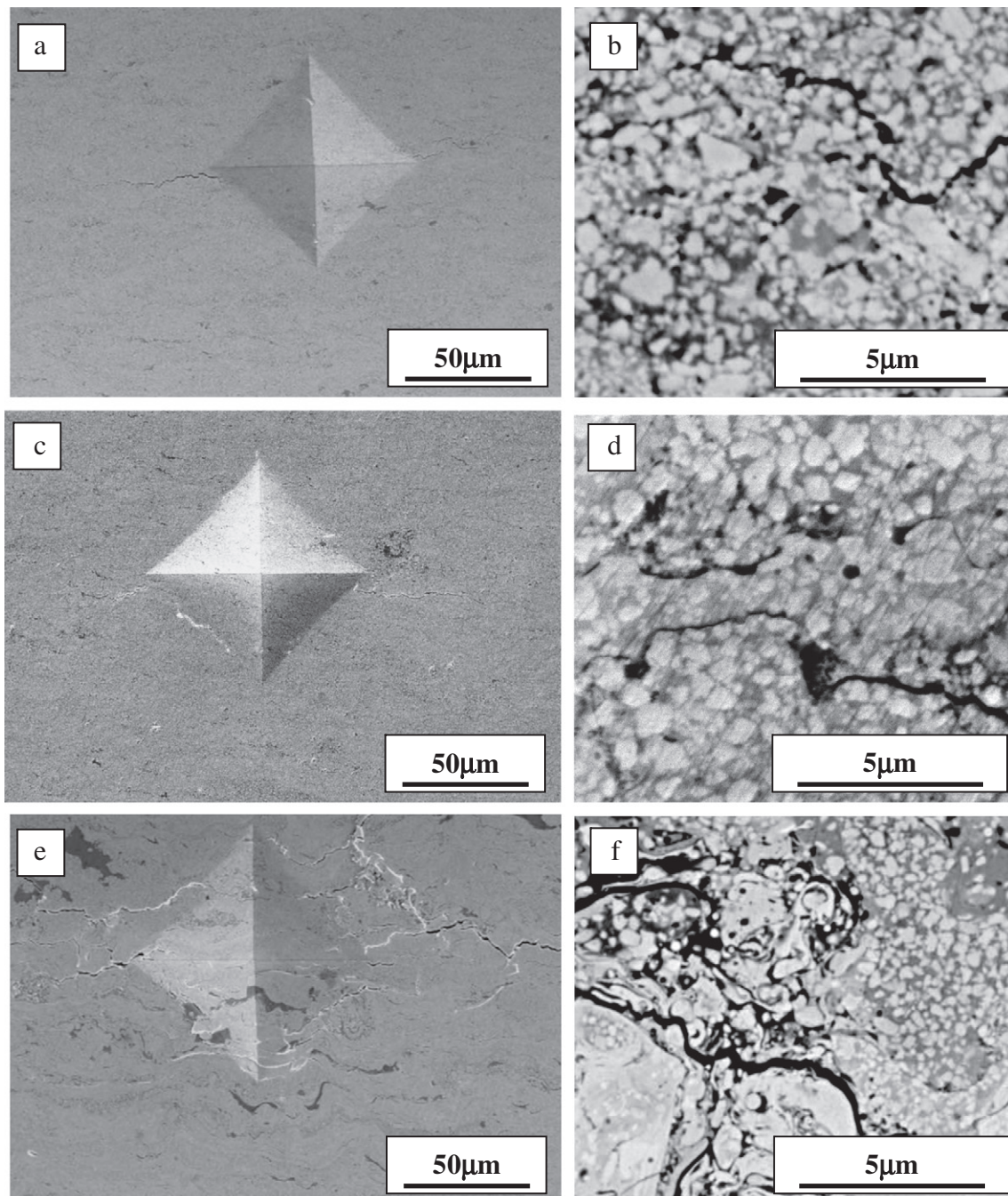


Fig. 4. Indentation and crack micrographs for the cross-sectional surfaces of the (a and b) AK coating, (c and d) JP coating, and (e and f) JK coating.

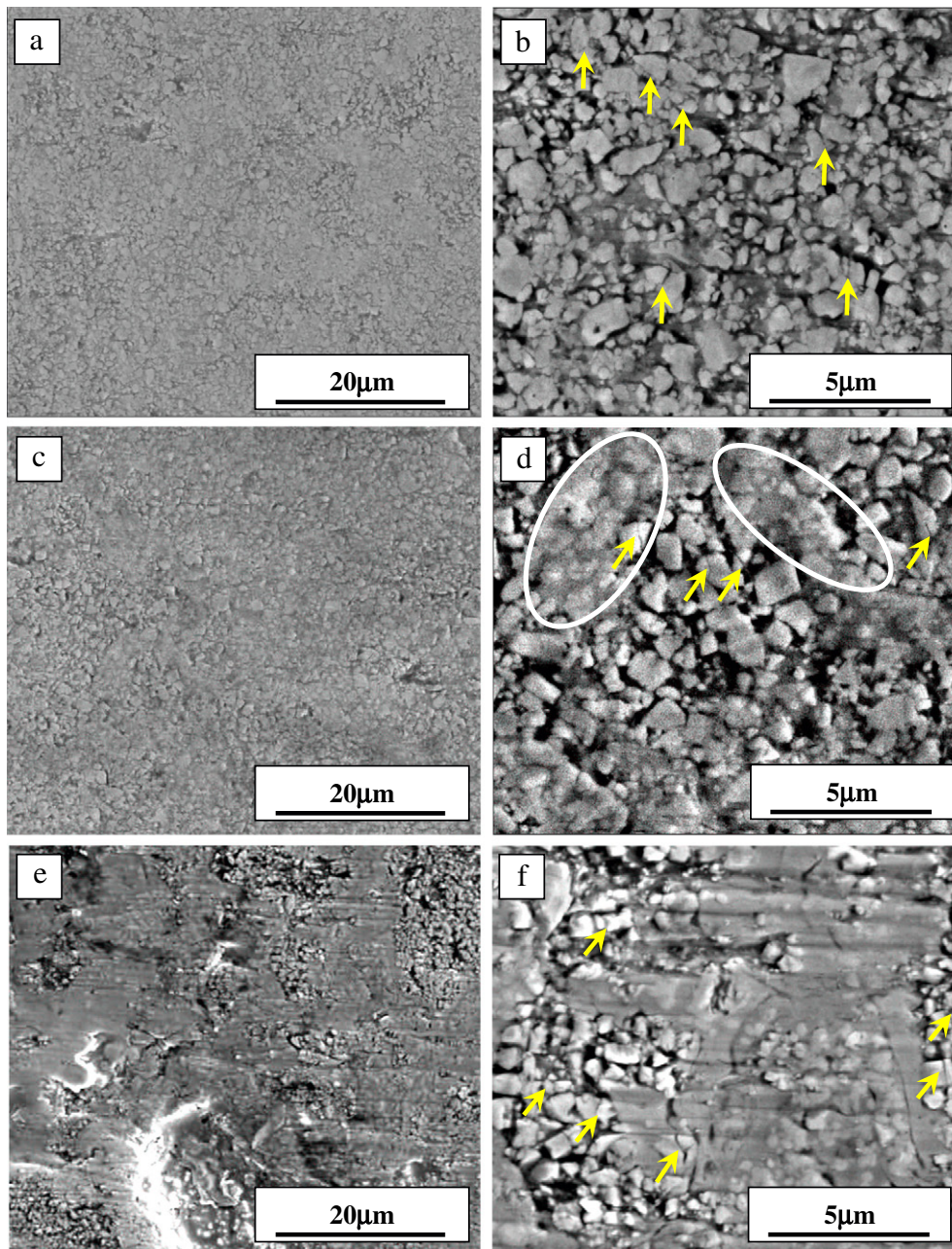


Fig. 5. Worn surface SEM images of the (a and b) AK, (c and d) JP and (e and f) JK coatings.

of the JK coating, and a different degree of exclusion and binder scratching around the WC particles as well as the different number of fractured WC particles (marked by arrows) could be observed on the high-magnification images of worn surfaces for the three coatings (Fig. 5b, d and f). Based on these typical worn surface morphologies, it can be concluded that the dominant wear mechanism of the JK coating was “micro-cutting” accompanied by delamination of the splats. Because the content of the high-hardness WC grains decreased while the content of the brittle phases such as W_2C , W and amorphous Co phase was increased in the more decarburized JK coating, this coating exhibited the lowest hardness and toughness. The JK coating with low hardness was relatively easy to cut with quartz abrasive during the abrasive wear test, while its poor toughness could result in the delamination of splats in the coating. The spray powder was deposited at a lower temperature flame for the AK coating, so the large number of WC particles was retained resulting in the higher coating hardness. Consequently, the widespread distribution of high-hardness WC

particles on the surface of the AK coating effectively hindered the penetration of the quartz abrasive, and the high toughness of the carbide coating could allow the binder absorb a part of energy generated by the abrasive attack with some degree of plastic deformation. The wear mechanisms, including the extrusion of the binder phase and its removal by plastic deformation and fatigue, carbide grain fracture and the undermining of the particles and subsequent particle pull-out were the dominant wear failure processes for the AK coating. The JP coating showed a much smaller degree of decarburisation than the JK coating, but a little more decarburisation than the AK coating, which caused the JP coating to exhibit a similar worn surface morphology and wear mechanisms to those of the AK coating.

Monticelli et al. [28] have reported that the moderate degree of decarburisation during the HVOF spraying of WC–Co leads to its improved resistance to abrasive wear. This characteristic is true for WC/Co(Cr) coatings deposited by the same spray gun, but not completely true for WC/Co(Cr) coatings produced with different

spray guns. For example, the AK coating deposited by the AK 07 HVAF spray gun without decarburisation exhibited higher wear resistance than the JP coatings deposited by the JP8000 HVOF spray gun, which showed only slight decarburisation in this study.

4.4. Sliding wear mechanism of the HVAF- and HVOF-sprayed WC-10Co4Cr coatings

The typical images of the worn surfaces of the AK, JP and JK coatings after sliding wear test are shown in Fig. 6.

As Fig. 6a, d and g shows, the AK coating had the smallest sliding trace width among the three coatings. Based on the high-magnification micrograph of the worn surfaces of the AK, JP and JK coatings, the AK coating exhibited the smoothest worn surface, with some shallow ploughs. There were also some dark regions (marked by arrows in Fig. 6b) on the worn surface of the AK coating, which were rich in Zr and O elements according to the EDS results shown in Fig. 6j, which could be attributed to the intrusion of the

ZrO₂ scraps. The phenomenon of ZrO₂ scraps squeezing into the coating surfaces was also found on the worn surfaces of the JP and JK coatings (marked by arrows in Fig. 6e, f, h and i). Because the AK coating high hardness effectively hindered the friction material (ZrO₂) from squeezing into its surface and its high toughness delayed the generation and propagation of fatigue cracks, the worn surface of the AK coating exhibited the smoothest morphology, without apparent cracks. The shallow ploughs on the wear surface were also attributed to this coating high toughness. The substantial amount of a very brittle binder matrix in the noticeably decarburized JK coating facilitated the generation of cracks under the repeated attacks of the ZrO₂ sliding sphere. Therefore, a large number of cracks and pits (generated by the delamination of the coating materials) were identified without apparent ploughs on the sliding worn surface of the JK coating (Fig. 6f). Those were attributed to coating low hardness and toughness and eventually resulted in the coating worst sliding wear resistance. A small number of shallow ploughs, pits and cracks (Fig. 6e) were found on the JP coating worn surface, which exhibited

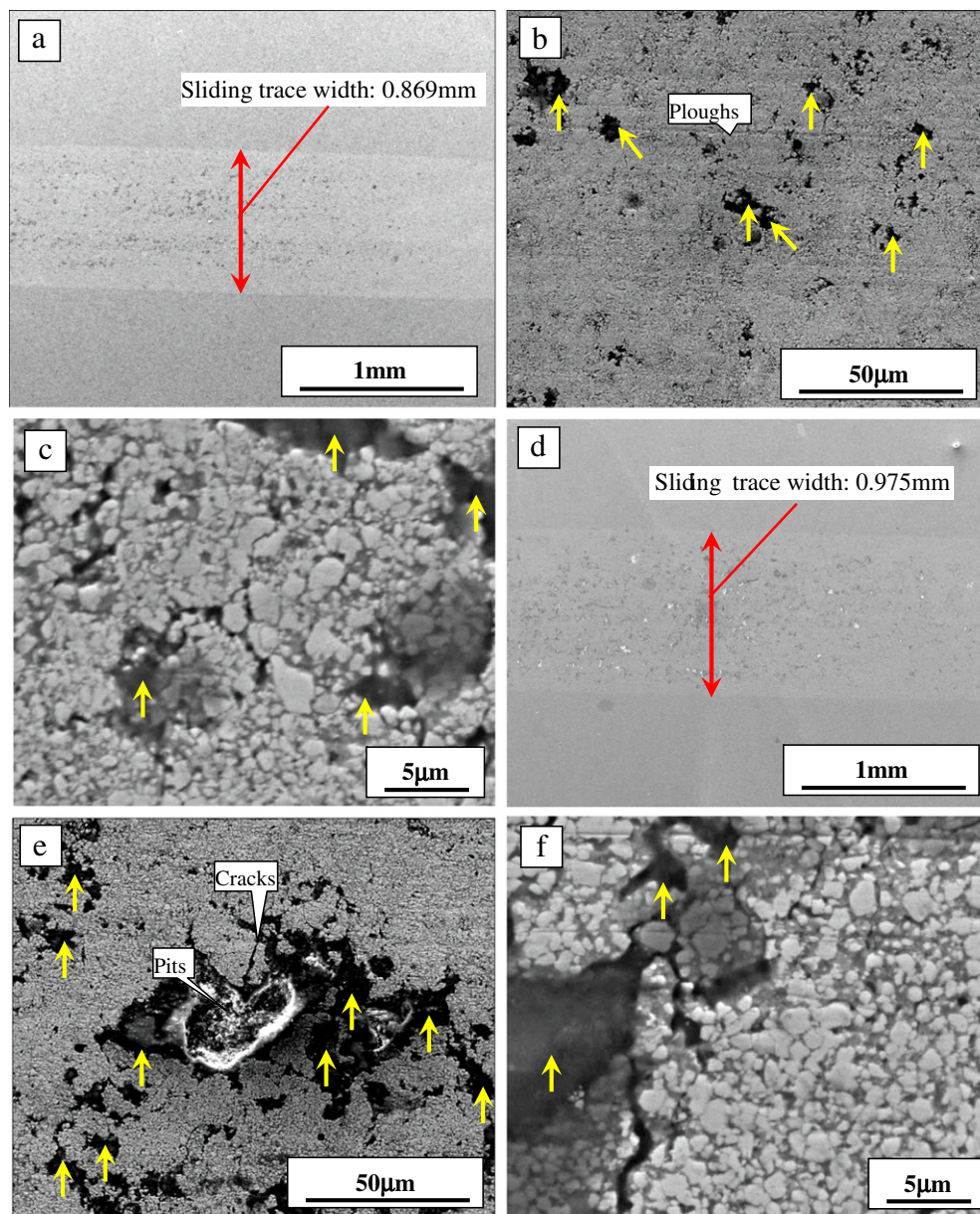


Fig. 6. Low, medium and high magnification images of the sliding worn trace morphology of the (a, b and c) AK, (d, e and f) JP, and (g, h and i) JK coatings, and (j) the typical EDS of the dark region marked by arrows.

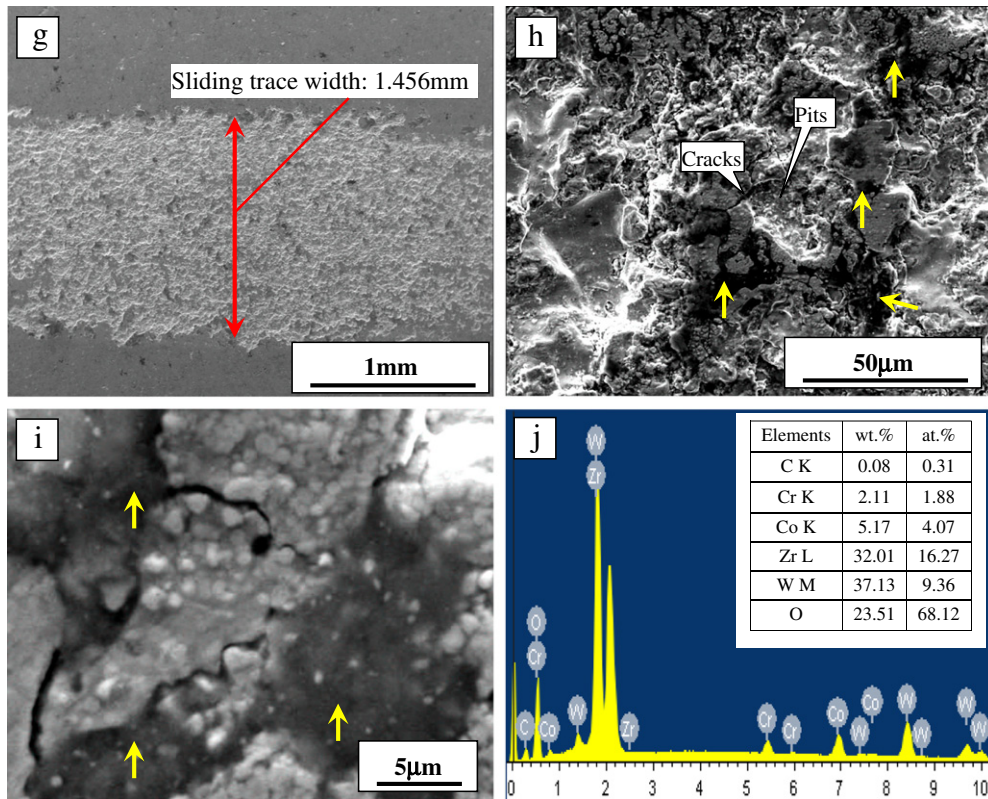


Fig. 6 (continued).

similarity to the wear defects found in both the AK and JK coatings. This reflected the fact that the JP coating resistance to sliding wear was in between that of the AK and JK coatings.

Based on the current analysis of the worn coating micrograph and the published results [26,27], the following wearing process was proposed. First, when two surfaces are brought into sliding contact, the Co/Cr binder phases between the WC particles undergo severe deformation. The deformed Co/Cr binder phases are extruded by the compressive stress of the protruding asperities of zirconia counter sphere. Next, the fatigue cracks generate and propagate under the repeated attack of the counter sphere without enough support from the Co/Cr binder, which leads to the pull-out of WC particles, spallation of splats and formation of the original wear debris. Some of the wear debris is carried away from the system, but some is entrapped between the contact surfaces. These entrapped debris particles cause further damage to both surfaces as a third-body abrasive, and the debris itself undergoes fragmentation during the sliding, which results in the formation of very fine debris particles [26].

The JK coating exhibited the lowest friction coefficient among the tested coatings (Table 3), which was attributed to its high brittleness and low hard WC phase content. The rapid spallation of coating materials and the lack of sufficient hard particles in the JK coating reduced the resistance of the coating materials to the movement of zirconia counter sphere, which was helpful in decreasing its friction coefficient during the sliding wear test. In case of the AK and JP coatings, the large number of remaining hard WC phase particles resisted to the movement of ZrO_2 spheres over the coating surfaces, which resulted in higher friction coefficients measured.

4.5. Electrochemical corrosion mechanism of the HVOF- and HVOF-sprayed WC-10Co4Cr coatings

The images of the AK, JP and JK coatings corrosion surfaces after anodic polarisation in 3.5 wt.% NaCl solution are shown in Fig. 7.

As Fig. 7 shows, the AK coating contained a large number of micro-cavities and some corrosion products on its corrosion surface. The JP coating surface had similar micro-cavities, but fewer corrosion products than the AK coating. There were only a small number of micro-cavities on the JK coating surface, which was mainly smooth, exhibiting very different morphology than the AK and JP coatings. The concept of matrix corrosion (the matrix near the hard particles was dissolved due to micro-galvanic effects) and subsequent release of the hard phase has always been considered the main corrosion mechanism of WC-based cermet materials [28,29]. However, recently some researchers [11,30] have proposed that the corrosion of both the WC (hard phase) and the matrix can take place simultaneously and result in the pull-out of the WC particles. According to the two corrosion mechanisms, the pull-out of the WC particles could not be avoided in WC-based cermet materials during the electrochemical corrosion process, which led to various numbers of micro-cavities being generated on the three coatings surfaces. The XRD analysis indicated that most of the Co/Cr binder phase in the AK coating was crystalline (Fig. 2), which resulted in the generation of the passive film in the form of a surface oxide in the coatings containing Cr, and partly suppressed the binder material dissolution into the solution of the AK coating, increasing its resistance to corrosion (Fig. 7b). Meanwhile, the other types of oxide films, such as WO_3 and CoO , were also generated and attached onto the Cr_2O_3 film. These corrosion products, in turn, protected the coating from severe corrosion attack. As for the JP coating, a part of the metal Co/Cr binder phase was amorphous according to the XRD (Fig. 2) and the intensive distribution of amorphous region marked by an ellipse in Fig. 7d showed a smoother surface with fewer micro-cavities than the other regions exhibiting high corrosion resistance. It also explained the smoothest corrosion surfaces in case of the JK coating that appeared with the largest amount of amorphous phase present (Fig. 2). Some studies [14,15] have also identified similar phenomena in which the amorphous Co–W–C alloys exhibit very high resistance to corrosion.

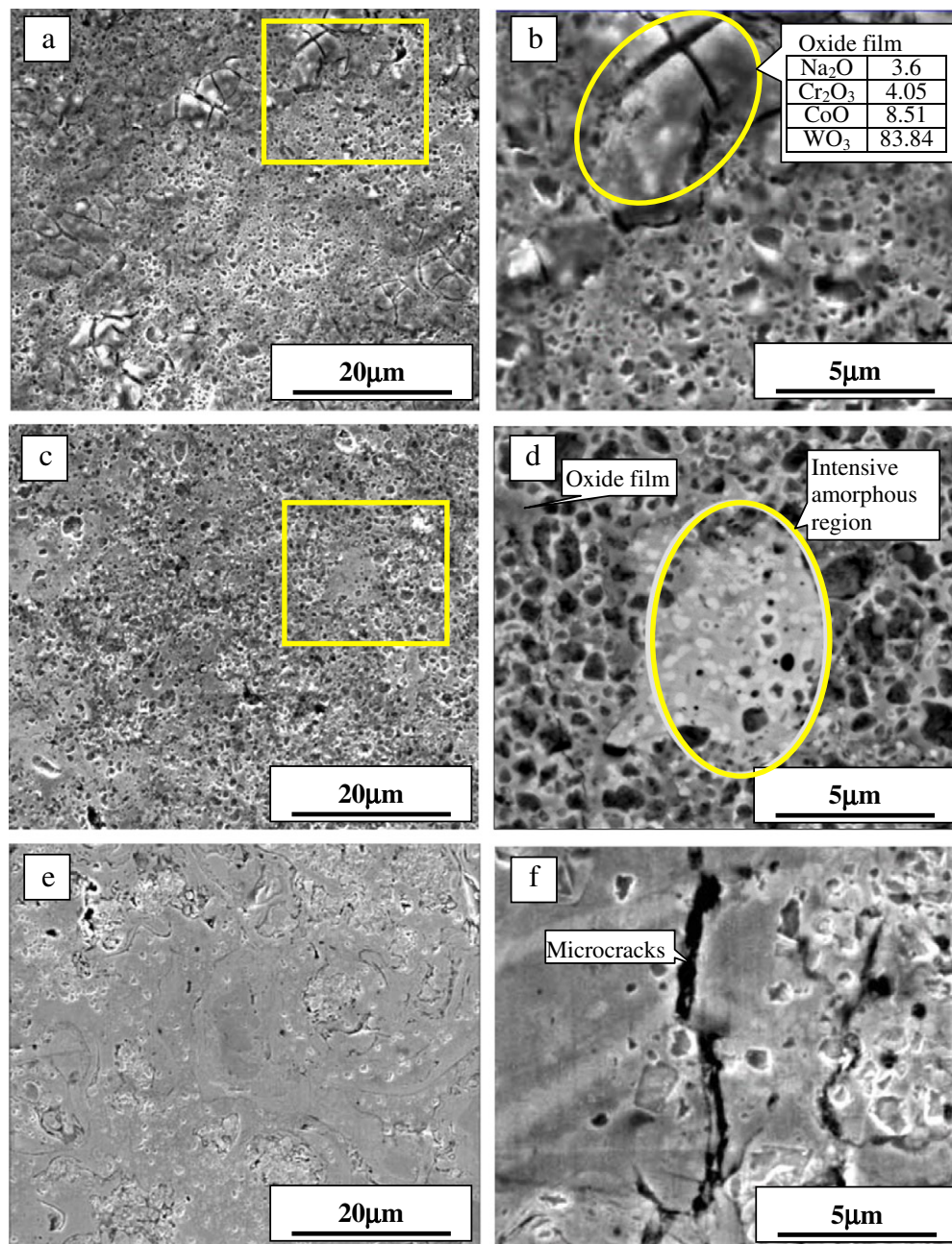


Fig. 7. Corrosion surfaces of the coatings after anodic polarisation in static 3.5 wt.% NaCl solution: (a and b) AK, (c and d) JP and (e and f) JK coatings.

Although the JK coating experienced the most severe decarburisation and contained the largest amount of amorphous phase, its overall corrosion resistance was inferior to that of the other two coatings due to the presence of micro-cracks, which acted as the infiltration paths for the solution (Fig. 7f). Other studies [31–33] have reported that the pores, especially penetrating pores in the coating, also exhibited a similar adverse effect on the corrosion resistance of the HVOF coating, so the JK coating's high porosity was also partly responsible for its poor corrosion resistance.

In summary, the AK coating exhibited the highest corrosion resistance, which was attributed to the crystalline Cr and its very dense microstructure without cracks. This fact could significantly affect the corrosion behaviour of WC coating layers in several ways. First, the open circuit potential difference between WC particles and binder materials causes micro-galvanic corrosion between the two phases in corrosive environments. The WC becomes cathodic and the binder

material becomes anodic, resulting in the corrosion of anodic binder materials. Second, WC particles are the main phase of WC-10Co4Cr coating materials. Considering the area ratio effect between large cathodes and small anodes, more severe micro-galvanic corrosion is likely to occur. Finally, the substrate material of low-carbon steel exhibited the lowest potential (−0.658 V). When the NaCl solution infiltrates along micro-cracks or pores existing in the coating, macro-galvanic corrosion is expected to occur at the coating/substrate interface [34]. It was found that the chemical composition of metallic binder materials, phase composition and control of microcracks and pores were the most important factors influencing the corrosion resistance of the HVOF/HVAF-sprayed WC cermet coatings in corrosion environments.

The average properties of the WC-10Co4Cr coatings deposited using standard parameters with a Jet Kote III spray gun were inferior to those deposited by the AK 07 HVAF and JP8000 HVOF systems, but it can hardly be said that the WC-10Co4Cr coating deposited by the

Jet Kote spray gun always exhibited poor performance. A significant amount of optimisation work should be performed on both the feedstock powder and the spraying parameters for this spraying system.

5. Conclusion

Three WC-10Co4Cr coatings were deposited by HVOF and HVAF processes and their microstructure and properties were investigated in this study. The following conclusions were drawn as a result.

- (1) The WC-10Co4Cr coating deposited by the HVAF spraying process exhibited nearly the same phase composition as its initial feedstock powder, which included mainly the WC and some $\text{Co}_3\text{W}_3\text{C}$ and crystal Co phases with nearly no decarburisation. The JK coating sprayed with Jet Kote III-HVOF equipment exhibited the most severe decarburisation with high-intensity W_2C and even metallic W phase. The phase composition of the JP coating deposited by the JP8000-HVOF system was composed of main WC and minor W_2C peaks and exhibited a light degree of decarburisation.
- (2) The wear resistance and mechanism of the HVOF/HVAF-sprayed coatings were influenced not only by their hardness but also by their fracture toughness. The high hardness of carbide coating could effectively hinder the cuts caused by the abrasives, and their high toughness could make the binder absorb some of the energy caused by abrasive attacks with some degree of plastic deformation.
- (3) The WC-10Co4Cr coatings, which had different degrees of decarburisation, exhibited different dominant wear mechanisms.
- (4) The electrochemical corrosion resistances and mechanisms of HVAF- and HVOF-sprayed WC-10Co4Cr coatings were influenced by their phase compositions and microstructures.

Acknowledgements

This research was supported by the Project of Training Targets of Young Key Teachers of Common College & University in Hunan Province, the Fundamental Research Funds for the Central University and the Projection of Young Teacher's Growth.

References

- [1] Q. Wang, Z.H. Chen, Z.X. Ding, *Tribol. Int.* 42 (7) (2009) 1046.
- [2] S.F. Wayne, S. Sarnpath, *J. Therm. Spray Technol.* 1 (4) (1992) 307.
- [3] Z. Yao, J. Stiglich, T.S. Sudarshan, *Met. Powder Rep.* 53 (2) (1998) 32.
- [4] L. Jacobs, M.M. Hyland, M.D. Bonte, *J. Therm. Spray Technol.* 8 (1) (1999) 125.
- [5] L. Jacobs, M.M. Hyland, M. De Bonte, *J. Therm. Spray Technol.* 7 (2) (1998) 213.
- [6] A. Verstak, V. Baranovski, in: B.R. Marple, M.M. Hyland, Y.-C. Lan, R.S. Lima, J. Voger (Eds.), *AC-HVAF Sprayed Tungsten Carbide: Properties and Applications*, Thermal Spray 2006: Building on 100 Years of Success, ASM International, Seattle, WA, May 15–18, 2006, (paper 11827).
- [7] A. Verstak, V. Baranovski, *Deposition of carbides by activated combustion HVAF spraying, thermal spray solutions: advances in technology and application*, May 10–14, 2004 (Osaka, Japan), DVS – German Welding Society, 2004, p. 551.
- [8] R.Q. Guo, C. Zhang, Q. Chen, Y. Yang, N. Li, L. Liu, *Corros. Sci.* 53 (7) (2011) 2351.
- [9] S.L. Liu, X.P. Zheng, G.Q. Geng, *Wear* 269 (5–6) (2010) 362.
- [10] S. Matthews, M. Hyland, B. James, *J. Therm. Spray Technol.* 13 (4) (2004) 526.
- [11] V.A.D. Souza, A. Neville, *J. Therm. Spray Technol.* 15 (1) (2006) 106.
- [12] Joan M. Perry, Anne Neville, Trevor Hodgkiess, *J. Therm. Spray Technol.* 11 (2002) 536.
- [13] M. Magnani, P.H. Suegama, N. Espallargas, S. Dosta, C.S. Fugivara, J.M. Guilemany, A.V. Benedetti, *Surf. Coat. Technol.* 202 (19) (2008) 4746.
- [14] H. Capel, P.H. Shipway, S.J. Harris, *Wear* 255 (2003) 917.
- [15] P.H. Shipway, L. Howell, *Wear* 258 (2005) 303.
- [16] Y. Ishikawa, J. Kawakita, S. Osawa, T. Itsukaichi, Y. Sakamoto, M. Takaya, S. Kuroda, *J. Therm. Spray Technol.* 14 (3) (2005) 384.
- [17] Q. Wang, L.X. Li, G.B. Yang, X.Q. Zhao, Z.X. Ding, *Surf. Coat. Technol.* 206 (19–20) (2012) 4000.
- [18] D.A. Stewart, P.H. Shipway, D.G. McCartney, *Acta Mater.* 48 (7) (2000) 1593.
- [19] M.S.A. Khan, T.W. Clyne, in: C.C. Berndt (Ed.), *Thermal Spray: Practical Solutions for Engineering Problems*, ASM International, Materials Park, Ohio, 1996, p. 113.
- [20] P. Aroto, L. Bartha, R. Porat, S. Berger, *A. Rosen, Nanostruct. Mater.* 10 (1998) 245.
- [21] B.H. Kear, G. Skandan, R.K. Sadangi, *Scr. Mater.* 44 (8–9) (2001) 1703.
- [22] J.R. Fincke, W.D. Swank, D.C. Haggard, *Proceedings of the 7th National Thermal Spray Conference*, ASM Int, Boston, 1994, p. 325.
- [23] C. Verdon, A. Karimi, J.L. Martin, *Mater. Sci. Eng., A* 246 (1–2) (1998) 11.
- [24] D. Zhang, S.J. Harris, D.G. McCartney, *Mater. Sci. Eng., A* 344 (1–2) (2003) 45.
- [25] P. Chivavibul, M. Watanabe, S. Kuroda, K. Shinoda, *Surf. Coat. Technol.* 202 (3) (2007) 509.
- [26] Q. Yang, T. Senda, A. Ohmori, *Wear* 254 (1–2) (2003) 23.
- [27] S.H. Zhang, T.Y. Cho, J.Ho. Yoon, M.X. Li, P.W. Shum, S.C. Kwon, *Mater. Sci. Eng. B* 162 (2) (2003) 127.
- [28] C. Monticelli, A. Frignani, F. Zucchi, *Corros. Sci.* 46 (5) (2004) 1225.
- [29] A. Trueman, D.P. Schweinsberg, G.A. Hope, *Corros. Sci.* 41 (7) (1999) 1377.
- [30] M. Takeda, N. Morihoro, R. Ebara, Y. Harada, *Mater. Trans.* 43 (11) (2002) 2860.
- [31] G. Bolelli, R. Giovanardi, L. Lusvardi, T. Manfredini, *Corros. Sci.* 48 (11) (2006) 3375.
- [32] P.H. Suegama, C.S. Fugivara, A.V. Benedetti, J. Fernández, J. Delgado, J.M. Guilemany, *Corros. Sci.* 47 (3) (2005) 605.
- [33] I.B. Singh, D.P. Mandal, M. Singh, S. Das, *Corros. Sci.* 51 (2) (2009) 234.
- [34] J.E. Cho, S.Y. Hwang, K.Y. Kim, *Surf. Coat. Technol.* 200 (8) (2006) 2653.